Thin Solid Films 558 (2014) 27–30

Contents lists available at ScienceDirect

Thin Solid Films

journal homepage: www.elsevier.com/locate/tsf

Effects of Y contents on surface, structural, optical, and electrical properties for Y-doped ZnO thin films

Sungeun Heo, Sanjeev K. Sharma, Sejoon Lee, Youngmin Lee, Changmin Kim, Byungho Lee, Hwangho Lee, Deuk Young Kim *

Department of Semiconductor Science, Dongguk University-Seoul, Seoul 100-715, Republic of Korea

ARTICLE INFO

Article history:
Received 11 September 2013
Received in revised form 1 February 2014
Accepted 5 February 2014
Available online 14 February 2014

Keywords:
Yttrium-doped zinc oxide
Thin films
Sol–gel deposition
Structural properties
Electrical properties
Photoluminescence

ABSTRACT

For the sol–gel synthesis of Y-doped ZnO (YZO) thin films, the mole concentration of Y significantly affects the physical properties of YZO. Namely, the incorporation of Y dopants into ZnO helps improve the surface, structural, optical, and electrical properties of YZO. When the appropriate concentration of Y is doped in YZO (i.e., Y ~ 2 at.%), the densities of oxygen-related native point defects are minimized, and the crystallite sizes of YZO grains are maximized. Consequently, the YZO (Y: 2 at.%) films show the improved electrical properties with the lower Hall resistivity.

1. Introduction

Wide energy band-gap semiconductor (~3.4 eV), zinc oxide (ZnO), has great potential for short wavelength optoelectronic devices because its large exciton binding energy (~60 meV at 300 K) enables stable excitonic emission at room temperature [1,2]. When ZnO is doped with extra foreign dopants, a spectrum of ZnO-based device applications can be extended toward various respects (e.g., transparent-conducting oxides [3–6], non-perovskite ferroelectric oxide [7–11], diluted magnetic semiconductors [12–18], and band gap-engineered materials [19–21]).

Among various extra foreign element-doped ZnO films, recently, Y-doped ZnO (YZO) has been of ample interest because Y improves the optical and the electrical properties of YZO [22–26]. For instance, Yang et al. [24] demonstrated tunable deep-level emission in YZO nanoparticles. Chen et al. [25] investigated the thermal stability of YZO films on GaN substrates. Kaur et al. [26] observed improved electrical conductivity from Y-doped ZnO films.

Compared to other techniques for the synthesis of YZO, a sol–gel method is much advantageous because of its simplicity, low cost, excellent homogeneity, and low process temperature [27–29]. In addition, the sol–gel process guarantees high purity of the product. In other words, since the sol–gel process allows the usage of highly-pure precursors with precise molar-fractions [30], the method renders high controllability to manipulate both the fraction of the solid state components and the size of the films [31,32]. Thus, the sol–gel technique is beneficial for the growth of high quality YZO.

In this study, we prepared YZO thin films by the sol–gel method and investigated the effects of the Y concentration on the surface, structural, optical, and electrical properties of the YZO thin films. The material properties are thoroughly examined upon the variation of the Y contents, and the correlationships between the intrinsic defects and the physical properties are discussed upon the variation of the Y concentration.

2. Experimental

YZO thin films were synthesized on *p*-type Si substrates by the sol–gel spin-coating technique. The sols were prepared by dissolving 0.5 M zinc-acetate-dihydrate ($Zn(CH_3COO)_2 \cdot 2H_2O$) in 2-methoxy-ethanol ($C_3H_8O_2$) at room temperature. Then, the solution was mixed by magnet stirring for 2 h at 60 °C to obtain transparent and clear solution. Yttrium-acetate-hydrate ($Y(CH_3COO)_2 \cdot H_2O$) was used as a dopant source (1, 2, 3, and 4 at.%). A stabilizing agent, monoethanolamine (MEA), was added drop-by-drop to the solution so as to completely eliminate the turbidity and the precipitates. Then, the solution became very clear, transparent, and homogenous. The solution was left to age for more than 24 h to obtain optimal viscosity. The substrates were ultrasonically cleaned by rinsing in 2-propanol, acetone, methanol, and deionized water for 15 min in each step. Thereafter, the prepared solution was spin-coated onto the *p*-Si substrates for 20 s at 3000 rpm. To evaporate the solvent and to remove the organic residues, the coated YZO layers were heated and cured at

* Corresponding author. Tel.: +82 2 2260 3802; fax: +82 2 2260 3945.
E-mail address: dykim@dongguk.edu (D.Y. Kim).

http://dx.doi.org/10.1016/j.tsf.2014.02.025
0040-6090/

300 °C for 10 min in an electric oven under atmospheric pressure. The above coating procedures were repeated by 5 cycles. To improve the crystal properties, thereafter, the YZO films were subsequently annealed at 500 °C for 3 min in vacuum by using rapid thermal annealing.

The surface and the cross-sectional microstructures of the YZO films were monitored by the field-emission scanning electron microscopy (FE-SEM) using a Hitachi-S-4700 system (Japan). The structure and the lattice phases of the films were characterized by X-ray diffraction (XRD) using a Rigaku-Ultima-IV system (Japan). The used radiation source was Cu K_α ($\lambda \sim 0.154$ nm), and the X-ray radiation was performed at 40 kV and 450 mA conditions. The chemical bonding states were examined by X-ray photoelectron spectroscopy (XPS) using a Multilab-2000 system (UK). For the calibration of binding-energy positions, the peak position of C 1s was used as the reference energy value. To investigate the optical properties, photoluminescence (PL) measurements were carried out at 300 K using an excitation source of a He–Cd laser (3250-Å line) and a 75-cm monochromator equipped with a GaAs photomultiplier tube. Electrical properties were measured by the standard *van der Pauw* Hall-effect method using an Ecopia-HMS-3000 system (Korea).

3. Results and discussion

Fig. 1 displays the surface and the cross-sectional SEM images of the sol–gel-synthesized YZO thin films (Y: 1 to 4 at.%). The films are composed of YZO grains with the average diameter of a few tens of nanometer. As the Y contents increase up to Y = 2 at.%, the mean grain size is increased. For the YZO thin film with Y of 2 at.%, the grains are closely packed, and the surface seems to be most uniform among the samples. The thickness of the YZO films is increased from 125 to 195 nm as the Y concentration increases (see each inset). The increase of the film thickness is attributed to the higher viscosity of the sol that contains a larger mole fraction of Y.

Fig. 2 shows the XRD patterns of the YZO thin films. All of the samples reveal a clear diffraction pattern of (0002) at the Bragg angle of $2\theta_{Bragg} \approx 33.1°$ and display no additional peaks from Y_2O_3 precipitates. This indicates that the Y dopants are well incorporated into the host lattice of ZnO though the samples were prepared on Si substrates at low temperature. The high crystal quality of the sol–gel-synthesized YZO films can be interpreted by the lower ionization energy of Y. In other words, the Y dopants having low ionization energy release the difference between the surface free energy of Si and the *c*-axis preference energy of ZnO. As a result, single-crystalline (0002) YZO could be easily grown on the Si substrate even without any catalyst such as Au [33].

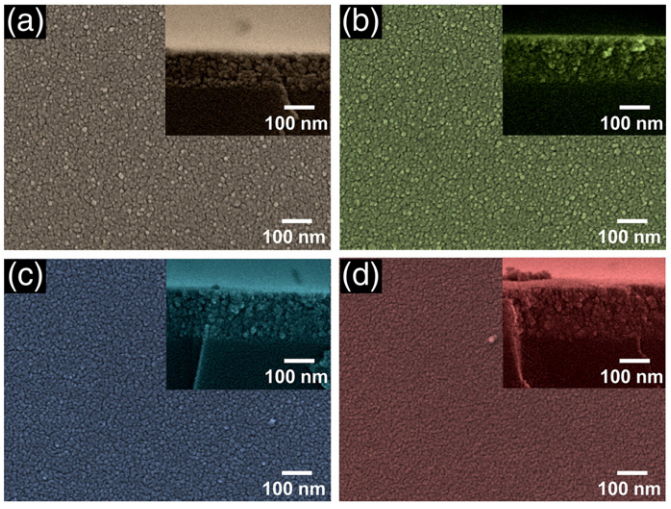

Fig. 1. SEM surface images of YZO thin films with different Y concentrations: (a) 1 at.%, (b) 2 at.%, (c) 3 at.%, and (d) 4 at.%. The inset of each figure displays the cross-sectional SEM image of the film represented in the figure.

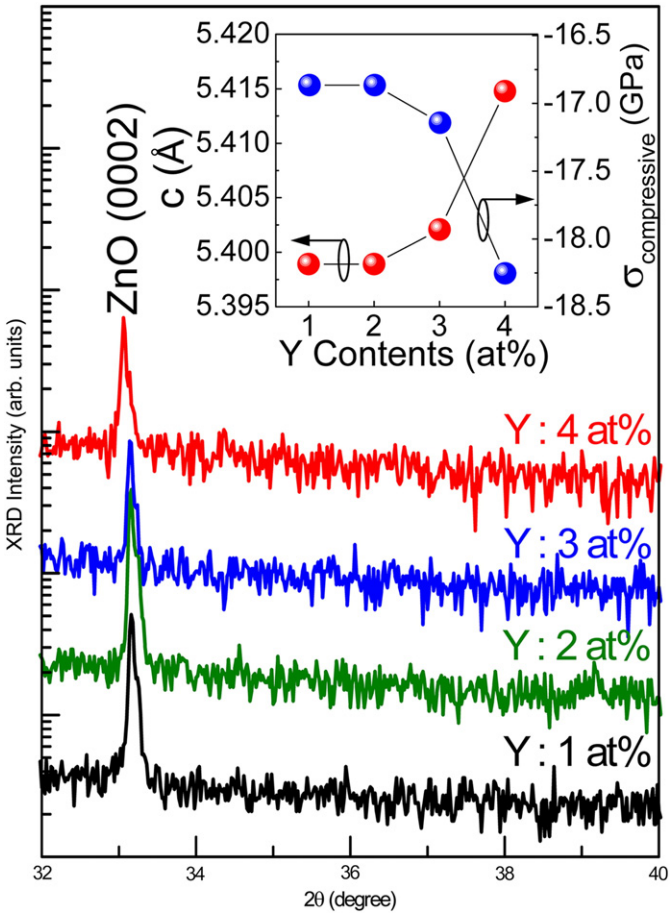

Fig. 2. XRD patterns of YZO thin films with different Y concentrations (Y: 1–4 at.%). The inset shows *c* and σ as a function of the Y concentration. The negative sign of σ indicates that the stress in the film is compressive in nature [21].

In our YZO films, the observed Bragg angles are smaller than that of bulk ZnO ($2\theta_{Bragg} = 34.42°$), and $2\theta_{Bragg}$ of YZO decreases as the Y concentration increases. This originates from the larger ionic radius of Y^{3+} (0.92 Å) than that of Zn^{2+} (0.74 Å) [34]. The incorporation of larger ionic dopants changes the lattice constant (c) and creates the residual stress (σ) in the film. By using Bragg's law [35], c_{YZO} is determined from 0.5399 to 0.5419 nm for the YZO films. The obtained c_{YZO} is greater than that of pure ZnO ($c_{ZnO} = 0.5207$ nm) [36] because the larger Y^{3+} ions substitute at the host Zn^{2+} lattice sites. In addition, c_{YZO} increases with increasing the Y contents (inset of Fig. 2). This gives rise to the increase in the residual stress of the film. As the Y dopant concentration increases, the magnitude of σ increases from |−16.866| to |−18.254| GPa, where σ was estimated from the deviation between c_{YZO} and c_{ZnO} (i.e., $\sigma = -E_{ZnO}(c_{YZO} - c_{ZnO}) / c_{ZnO}$, E_{ZnO}: Young's modulus of ZnO).

After confirming the substitution of Y dopants into host material ZnO, we examined the chemical bonding states of the solid-state species in YZO. Fig. 3 shows the XPS survey spectra of the YZO films (Y = 1–4 at.%). The XPS peaks from the main lattice components of Zn (3p, $2p_{3/2}$, $2p_{1/2}$), O (1s), and Y (3d) are visible. Except for several Auger recombination peaks, no additional signals from other contaminants are observable. These depict a high purity of the sol–gel-synthesized YZO films.

Due to the small amount of Y dopants, however, the peak from the Y 3d core level is weak. For more clarity on the presence of Y ions in YZO, thus, we carried out high-resolution XPS measurements. Main features occur at ~158 eV, and the spectrum can be distinguished by two Gaussian peaks of $3d_{3/2}$ and $3d_{5/2}$ (inset of Fig. 3). This verifies the incorporated Y dopants to be in a 3+ valence state [37]. According to Ingo et al. [38], for Y_2O_3, Y $3d_{3/2}$ and $3d_{5/2}$ were observed at 157.4 and

156.6 eV, respectively. In our YZO sample, however, Y 3d core levels appear at the increased binding-energy positions (i.e., Y $3d_{3/2}$ at 160.2 eV and $3d_{5/2}$ at 158.2 eV). The discrepancies arise from different Y–O bond lengths in between Y_2O_3 and YZO crystal lattices; hence, the result corroborates our YZO to contain no Y_2O_3 precipitates.

Since the incorporated Y^{3+} ions substitute at the Zn^{2+} sites in the ZnO host lattices, Y dopants may also affect the bonding properties of Zn and O host elements. In other words, the average bond-length of Zn–O is increased when doping bigger Y^{3+} ions into smaller Zn^{2+} ion sites (see also Fig. 2). Hence, the binding energies of Zn and O should be altered. Fig. 4 shows the XPS spectra of Zn 2p core levels for YZO films (left-hand-side panel). For YZO (1 at.%), the peaks of Zn $2p_{1/2}$ and Zn $2p_{3/2}$ appear at 1045 and 1022 eV, respectively. As the Y concentration increases, the peaks are shifted toward the lower energy region. This is indicative of the decrease in the bond strength of Zn, particularly, for the YZO films having the higher concentration of Y.

The right-hand-side panel of Fig. 4 displays the XPS spectra of O 1s core levels. In all samples, three types of oxygen bonds are observed near 529–534 eV. The Gaussian curves assigned as O_I, O_{II}, and O_{III} correspond to covalent bonds of O^{2-} ions with cations, natural oxygen atoms, and loosely-bound oxygen ions near the surface, respectively [39–41]. When the Y concentration is increased, the samples exhibit an identical tendency that the portion of O_{II} increases, whereas that of O_{II} and O_{III} decreases. For YZO with Y = 2 at.%, O_I is biggest and O_{II} is lowest. This implies that ZnO has a limited Y solubility [26].

In host material ZnO, oxygen-related bonds create deep-level energy states, and they play a crucial role for deep level emission [42]. To study the optical properties of YZO, thus, we measured the PL properties of the samples. The YZO films reveal strong ultra-violet emission with two deep-level emission peaks (Fig. 5). P_1 originates from near-band-edge emission, P_2 stems from oxygen antisites (O_{Zn}), and P_3 arises from oxygen interstitials (O_i) [43,44]. Regardless of the Y contents, P_1 is strong enough to verify high crystal quality of the YZO films. However, the portions of P_2 and P_3 are slightly altered when the doping concentration of Y is varied. P_2 and P_3 are decreased when the Y concentration is increased from 1 to 2 at.%, and those are increased again when the Y concentration exceeds 3 at.%. This might be related to the solution limit of Y, as observed in XPS measurements (see also Fig. 4).

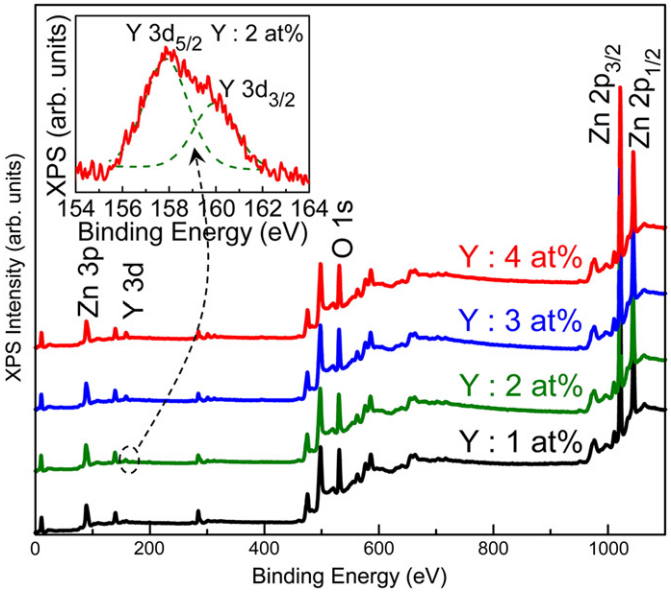

Fig. 3. XPS spectra of YZO thin films with different Y concentrations (Y: 1–4 at.%). A peak at 284.5 eV, arising from C 1s, was used as a reference binding-energy position for XPS measurements. The inset shows the high-resolution XPS spectrum of the Y 3d core level for the YZO (Y: 2 at.%) thin film.

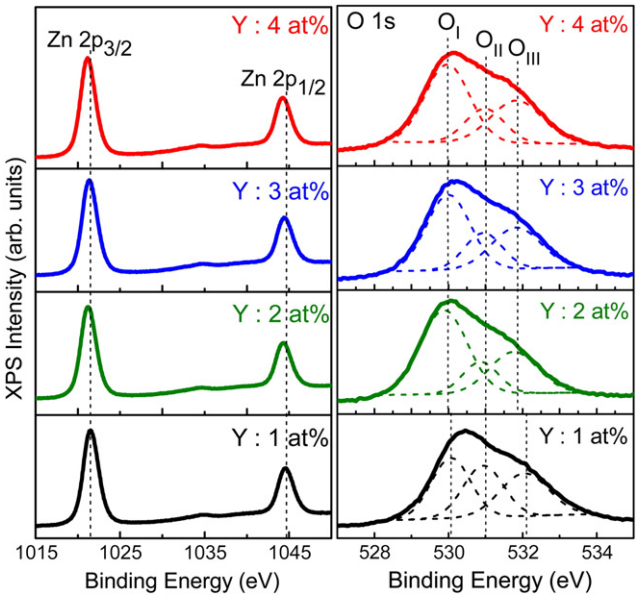

Fig. 4. High-resolution XPS spectra of Zn 2p (left-hand-side panel) and O 1s (right-hand-side panel) core levels for the YZO thin films (Y: 1–4 at.%).

Native defects, O_{Zn} and O_i, act as acceptors [45], while Y^{3+} dopants act as donors [46]. Therefore, the variation of P_2 and P_3 should definitely affect the electrical properties of YZO. To confirm the above hypothesis, we performed Hall-effect measurements at room temperature. Fig. 6(a) shows the carrier concentration (n) and resistivity (ρ) as a function of the Y concentration. The samples exhibit n-type semiconducting properties because of Y-doping. As can be expected from the results of

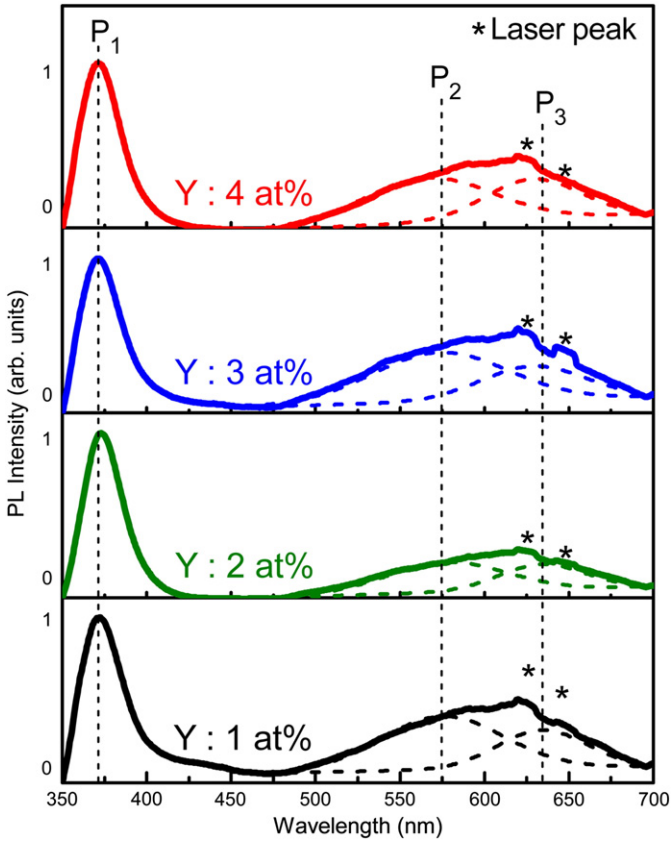

Fig. 5. PL spectra of YZO thin films (Y: 1–4 at.%) at 300 K. The PL intensity in each spectrum was normalized to unity by the maximum intensity of UV emission.

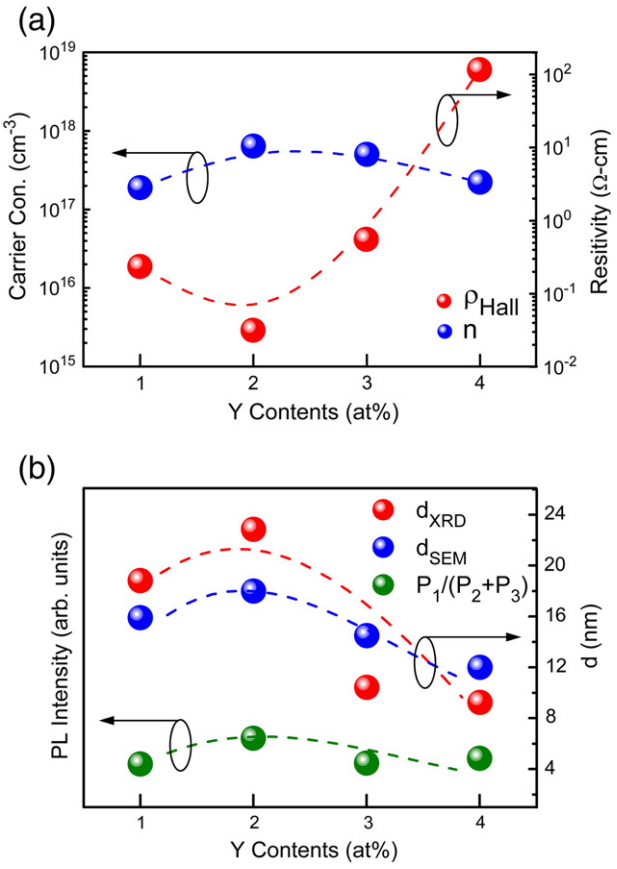

Fig. 6. (a) Carrier concentration and Hall resistivity as a function of the Y concentration. (b) PL intensity ratio of $P_1/(P_2 + P_3)$ and mean grain sizes as a function of the Y concentration. The mean grain sizes, d_{SEM} and d_{XRD}, were determined from SEM images and XRD data, respectively. In the case of d_{XRD}, we used a Scherrer formula [12].

XPS and PL, the magnitude of n is maximized at Y = 2 at.%. The lowest n is recorded in the YZO film with Y of 1 at.% ($n = 1.90 \times 10^{17}$ cm^{-3}), and the highest n is observed in the YZO film with Y of 2 at.% ($n = 6.42 \times 10^{17}$ cm^{-3}).

Here, it should be noted that ρ of YZO (Y: 2 at.%) is significantly decreased in spite of the little increase of n. Namely, ρ is decreased by more than one order of magnitude, although n is increased by a factor of ~3. This can be explained by the increased grain size (d) in YZO (Y: 2 at.%); i.e., the lattice distribution in solid-state materials is closely associated with the carrier mobility (μ). The magnitude of ρ is given by $\rho = 1/qn\mu$, where q is the standard quantity of the electronic charge [47]. In thin film materials, μ is mostly dominated by grain boundary scattering because the large number of free carriers are populated from point defects at the surfaces of the grain boundaries [5]. Thus, one can expect that decreased ρ for YZO (Y: 2 at.%) is associated with the increase in d of the film. As shown in Fig. 6(b), d of YZO is maximized at Y = 2 at.%, whereas the variation of $P_1/(P_2 + P_3)$ is insignificant. The trends are almost consistent with those of n and ρ. Therefore, we can conclude that decreased ρ comes from increased d due to the incorporation of Y.

4. Conclusions

YZO films were prepared on p-Si substrates by the sol–gel synthesis method. Due to the low ionization energy of Y, high quality YZO films were obtained despite of the low temperature growth process. The samples displayed the solution limit of Y dopants up to 2 at.%, and the YZO film with Y = 2 at.% revealed the lowest electrical resistivity among our samples. The decreased electrical resistivity was confirmed to originate from both the decreased density of positively-charged native-point-defects and the increased crystallite size of YZO. The incorporation of an appropriate concentration of Y helps improve the structural and the electrical properties of YZO.

Acknowledgments

This research was supported by the National Research Foundation of Korea through the Leading Foreign Research Institute Recruitment Program (NRF-2013-044975) and the Brain Korea 21$^+$ Program (22A20130000037) funded by the Korean Government's Ministry of Education (MoE).

References

[1] X. Fang, J. Li, D. Zhao, D. Shen, B. Li, X. Wang, J. Phys. Chem. C 113 (2009) 21208.
[2] M. Willander, M.Q. Israr, J.R. Sadaf, O. Nur, Nanophotonics 1 (2012) 99.
[3] Y.-S. Kim, W.-P. Tai, Appl. Surf. Sci. 253 (2007) 4911.
[4] W. Yang, Z. Liu, D.-L. Peng, F. Zhang, H. Huang, Y. Xie, Z. Wu, Appl. Surf. Sci. 255 (2009) 5669.
[5] Y. Lee, C. Lee, E. Shim, E. Jung, J. Lee, D.Y. Kim, S. Lee, D. Fu, H.D. Yoon, J. Korean Phys. Soc. 59 (2011) 2774.
[6] Y. Lee, D.Y. Kim, S. Lee, J. Korean Phys. Soc. 60 (2012) 99.
[7] M. Joseph, H. Tabata, T. Kawai, Appl. Phys. Lett. 74 (1999) 2534.
[8] Dhananjay, J. Nagaraju, S.B. Krupanidhi, J. Appl. Phys. 101 (2007) 104104.
[9] M.D. Glinchuk, E.V. Kirichenko, V.A. Stephanovich, B.Y. Zaulychny, J. Appl. Phys. 105 (2009) 104101.
[10] Y. Lee, D.Y. Kim, S. Lee, D. Fu, J. Korean Phys. Soc. 60 (2012) 1891.
[11] S. Lee, Y. Lee, D.Y. Kim, T.W. Kang, J. Appl. Phys. 114 (2013) 064102.
[12] S. Lee, T.W. Kang, D.Y. Kim, J. Cryst. Growth 284 (2005) 6.
[13] S. Lee, Y. Shon, S.-W. Lee, S.J. Hwang, H.S. Lee, T.W. Kang, D.Y. Kim, Appl. Phys. Lett. 88 (2006) 212513.
[14] S. Lee, D.Y. Kim, Y. Shon, C.S. Yoon, Appl. Phys. Lett. 89 (2006) 022120.
[15] S. Lee, Y. Shon, T.W. Kang, C.S. Yoon, E.K. Kim, D.Y. Kim, Appl. Phys. Lett. 93 (2008) 022113.
[16] S. Lee, Y. Shon, D.Y. Kim, T.W. Kang, C.S. Yoon, Appl. Phys. Lett. 96 (2010) 042115.
[17] S. Lee, Y. Lee, Y. Shon, D.Y. Kim, T.W. Kang, Appl. Phys. Lett. 97 (2010) 182103.
[18] C.O. Kim, S. Kim, H.T. Oh, S.-H. Choi, Y. Shon, S. Lee, H.N. Hwang, C.-C. Hwang, Physica B 405 (2010) 4678.
[19] F. Bertram, S. Giemsch, D. Forster, J. Christen, R. Kling, C. Kirchner, A. Waag, Appl. Phys. Lett. 88 (2006) 061915.
[20] M.K. Yadav, M. Ghosh, R. Biswas, A.K. Raychaudhuri, A. Mookerjee, S. Datta, Phys. Rev. B 76 (2007) 195450.
[21] C.-L. Tsai, M.-S. Wang, Y.-H. Chen, H.-C. Chang, C.-J. Liu, C.-T. Lee, Y.-T. Shih, H.-J. Huang, Y.-J. Lin, J. Appl. Phys. 107 (2010) 113717.
[22] X. Han, K. Han, M. Tao, J. Electrochem. Soc. 157 (2010) H593.
[23] P.-T. Hsieh, R.W.-K. Chuang, C.-Q. Chang, C.-M. Wang, S.-J. Chang, J. Sol-Gel Sci. Technol. 58 (2011) 42.
[24] J. Yang, R. Wang, L. Yang, J. Lang, M. Wei, M. Gao, X. Liu, J. Cao, X. Li, N. Yang, J. Alloys Compd. 509 (2011) 3606.
[25] P. Chen, W. Lai, L.-C. Peng, C. Kuo, C.-L. Yeh, J. Sheu, C. Tun, IEEE Trans. Electron Devices 57 (2010) 134.
[26] R. Kaur, A. Singh, R. Mehra, Phys. Status Solidi (a) 202 (2005) 1053.
[27] T. Jun, K. Song, Y. Jung, S. Jeong, J. Moon, J. Mater. Chem. 21 (2011) 13524.
[28] S.-S. Li, Z. Zhang, J.-Z. Hang, X.-P. Feng, R.-X. Liu, Chin. Phys. B 20 (2011) 127102.
[29] H.-C. Hsu, H.-Y. Huang, M.O. Eriksson, T.-F. Dai, P.-O. Holtz, Appl. Phys. Lett. 102 (2013) 013109.
[30] C.-T. Wu, J.-J. Wu, J. Mater. Chem. 21 (2011) 13605.
[31] L. Znaidi, Mater. Sci. Eng. B 174 (2010) 18.
[32] A.B. Djurišić, X. Chen, Y.H. Leung, A.M.C. Ng, J. Mater. Chem. 22 (2012) 6526.
[33] Y. Zhang, G. Sun, H. Zhao, J. Li, Z. Zheng, Phys. Scr. 84 (2011) 045402.
[34] Q. Yu, W. Fu, C. Yu, H. Yang, R. Wei, Y. Sui, S. Liu, Z. Liu, M. Li, G. Wang, J. Phys. D. Appl. Phys. 40 (2007) 5592.
[35] B.B. He, Two Dimensional X-ray Diffraction, Wiley, Hoboken, 2009.
[36] R. Heller, J. McGannon, A. Weber, J. Appl. Phys. 21 (1950) 1283.
[37] J. Chastain, J.F. Moulder, Physical Electronics Division, Perkin-Elmer Corp, Eden Prairie, MN, 1992.
[38] G. Ingo, E. Paparazzo, O. Bagnarelli, N. Zacchetti, Surf. Interface Anal. 16 (1990) 515.
[39] R. Zhang, L. Fan, Y. Fang, S. Yang, J. Mater. Chem. 18 (2008) 4964.
[40] Y. Jin, Q. Cui, G. Wen, Q. Wang, J. Hao, S. Wang, J. Zhang, J. Phys. D. Appl. Phys. 42 (2009) 215007.
[41] J. Lang, Q. Han, J. Yang, C. Li, X. Li, L. Yang, Y. Zhang, M. Gao, D. Wang, J. Cao, J. Appl. Phys. 107 (2010) (074302-074302-074304).
[42] S.-S. Chang, C.H. Park, S.W. Park, Mater. Chem. Phys. 79 (2003) 9.
[43] X. Wei, B. Man, M. Liu, C. Xue, H. Zhuang, C. Yang, Physica B 388 (2007) 145.
[44] J. Zheng, J. Song, Q. Jiang, J. Lian, Appl. Surf. Sci. 258 (2012) 6735.
[45] B. Lin, Z. Fu, Y. Jia, Appl. Phys. Lett. 79 (2001) 943.
[46] M. Gao, J. Yang, L. Yang, Y. Zhang, J. Lang, H. Liu, H. Fan, Y. Sun, Z. Zhang, H. Song, Superlattice. Microst. 52 (2012) 84.
[47] D.K. Schroder, Semiconductor Material and Device Characterization, 3rd ed. Wiley, New York, 2006.